(Received 17 September 2024, Accepted 16 October 2024, Scheduled 28 October 2024)

A Compact UHF RFID Tag Antenna with Tunable Double Interdigitated Structures

Luoxin Cai[1], Zibin Shi[2], Yanwei Qiu[2], and Jiade Yuan[1,*]

[1] College of Physics and Information Engineering, Fuzhou University, Fuzhou 350300, China
[2] Xindeco IOT, Xiamen 361000, China

ABSTRACT: A compact and tunable ultra-high frequency (UHF) radio frequency identification (RFID) tag antenna is proposed. The antenna comprises a rectangular ring, two symmetrical radiating arms formed by multiple L-shaped stubs, and two interdigitated structures. By adjusting the parameters of double interdigitated structures, the resonant frequency of the antenna can be tuned coarsely and finely, while maintaining a nearly constant maximum power transmission coefficient. The proposed tag antenna has a size of 28 mm × 16 mm ($0.086\lambda \times 0.049\lambda$ at 920 MHz). Measurement results show that the proposed antenna can achieve the maximum reading distance of 6.8 m at 920 MHz under the condition of 3.28 W effective isotropic radiated power. The proposed RFID tag antenna offers several advantages, including compact size and frequency tunability, making it well suited for various RFID system applications.

1. INTRODUCTION

Ultra-high frequency (UHF) radio frequency identification (RFID) technology, a non-contact automatic identification method, has been widely adopted across various fields, including healthcare, inventory management, agriculture, and animal husbandry [1–5]. Its popularity stems from its key advantages: long read range, high data transfer rate, and large storage capacity. A passive UHF RFID system typically comprises three main components: a reader, a tag, and a computer system [6]. The tag itself consists of an antenna and a chip, with the chip storing information about the target object and the antenna responsible for receiving and transmitting electromagnetic waves [7]. As such, the tag plays a critical role in an RFID system, as its performance directly impacts the overall effectiveness of the system.

The miniaturization of tag antennas has long been a key area of research in UHF RFID technology, as smaller tags reduce production costs and expand the range of potential application scenarios. Several techniques have been developed to achieve this miniaturization. For instance, fractal meandering technology, as explored in [8–10], employs fractal geometries like the Koch and Hilbert curves due to their unique fractional dimensional properties. This allows the extension of the antenna's electrical length while maintaining a compact physical size, although it adds complexity to the design process. Another approach, described in [11, 12], reduces antenna size by utilizing substrates with high dielectric constants. While this method is efficient and straightforward, it increases material costs, making it less cost-effective. Ref. [13] addresses miniaturization by adjusting the capacitance of external lumped components, which successfully minimizes antenna size but complicates the fabrication process. In addition to these techniques, serrations, slots, slits, and stubs are often combined with patch antennas to achieve miniaturization in the design of anti-metal tag antennas [14, 15]. These miniaturized tag antennas can be roughly classified into two categories: flexible and rigid. Flexible tags offer several advantages over rigid tags, including enhanced conformability to various surfaces and lighter weight. These features allow flexible antennas to be used in diverse applications, such as wearable technology and curved surfaces [1].

Electrically small tag antennas often require multiple, simple tuning mechanisms. Ideally, the antenna should provide both coarse and fine tuning options for adjusting the resonant frequency [16]. Therefore, in this paper, a novel compact UHF RFID tag antenna based on double interdigitated structures is proposed. Compared to the aforementioned miniaturization techniques, the proposed antenna achieves miniaturization simply by appropriately meandering the radiating arms and embedding the interdigitated structures. When considering the entire process from design to fabrication, it is relatively simple. The antenna incorporates nonuniform interdigitated structures, enabling both coarse and fine tuning without significantly compromising the power transmission coefficient. This tuning method offers greater flexibility and practicality compared to the continuous embedding of identical interdigitated structures described in [17, 18].

2. ANTENNA STRUCTURE AND ANALYSIS

2.1. Antenna Structure

The proposed antenna consists of a rectangular feed ring, a pair of symmetrical meandered dipole arms, and two interdigitated structures. These interdigitated structures are positioned between the left and right dipole arms, as illustrated in Figure 1. The upper structure is referred to as Interdigitated Structure I,

* Corresponding author: Jiade Yuan (yuanjiade@fzu.edu.cn).

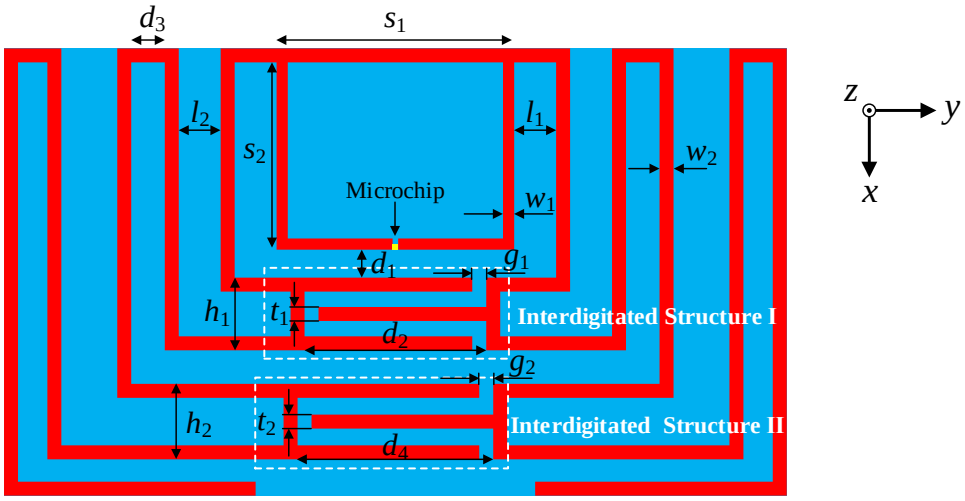

FIGURE 1. Configuration of the proposed tag antenna.

TABLE 1. Optimized parameters of the proposed tag antenna.

Parameter	Dimension (mm)	Parameter	Dimension (mm)	Parameter	Dimension (mm)	Parameter	Dimension (mm)
s_1	8.5	l_1	1.5	d_3	1.2	t_1	0.5
s_2	6.7	l_2	1.5	d_4	7	t_2	0.5
w_1	0.4	d_1	1	h_1	2.6	g_1	0.5
w_2	0.5	d_2	6.5	h_2	2.7	g_2	0.5

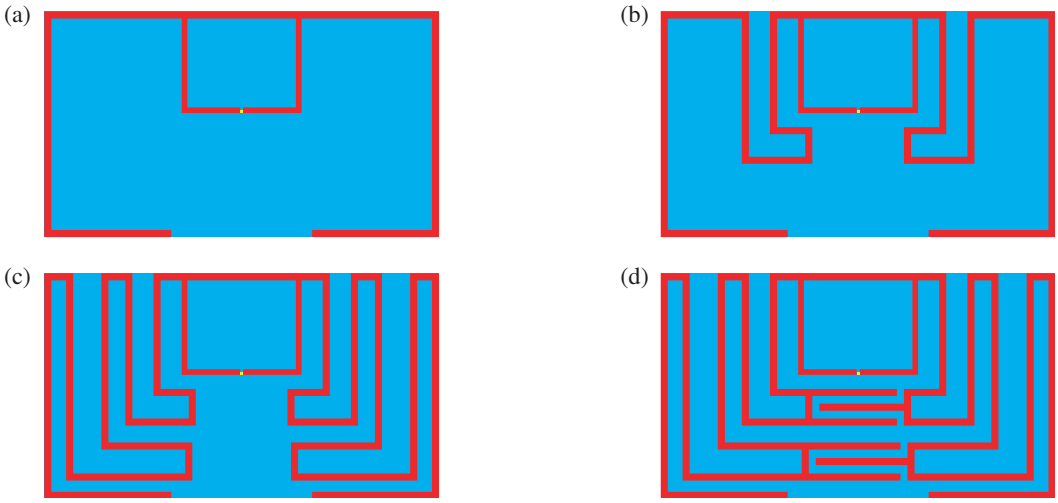

FIGURE 2. Structural evolution of the tag antenna design: (a) Antenna I, (b) Antenna II, (c) Antenna III, and (d) Antenna IV.

while the lower one is named Interdigitated Structure II. Each interdigitated structure contains three open stubs. The parameters for both Interdigitated Structure I and II are defined as follows: h_1 and h_2 represent the height; d_2 and d_4 denote the length; t_1 and t_2 indicate the width of the stubs; g_1 and g_2 specify the width of the end gaps, respectively. The antenna is printed on the substrate of the flexible PET with a thickness of 0.05 mm. The tag chip positioned in rectangular ring is MW8112 from MAXWAVE MICRO Co., Ltd., which has a reading sensitivity of -20 dBm and an impedance of $13.72 - j221.01\,\Omega$ at 915 MHz considering the effect of parasitic capacitance [19].

The proposed tag antenna is designed and analyzed by using Ansys high frequency structure simulator (HFSS). The optimized values of proposed antenna parameters are shown in Table 1.

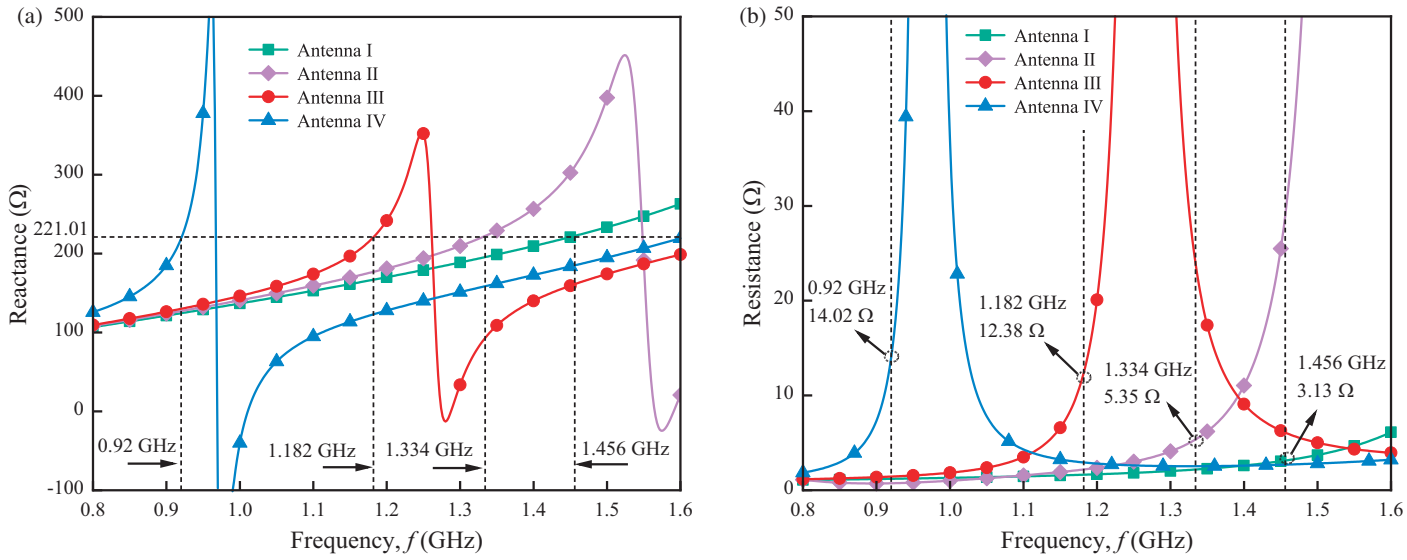

FIGURE 3. Input impedances of tag antennas in the evolution process. (a) Reactance. (b) Resistance.

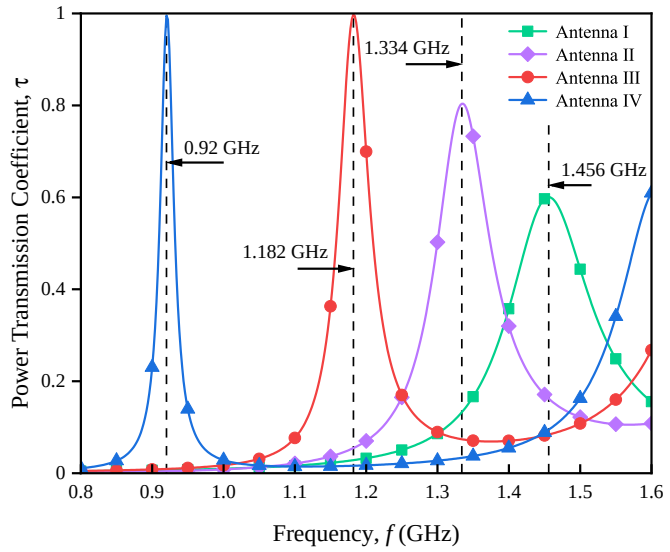

FIGURE 4. Power transmission coefficients of tag antennas in the evolution process.

2.2. Design Analysis

The power transmission coefficient is determined by impedances of tag antenna and tag chip as follows Equation (1) [20]:

$$\tau = \frac{4R_aR_c}{|Z_a + Z_c|^2} \tag{1}$$

where $Z_a = R_a + jX_a$ and $Z_c = R_c + jX_c$ are the antenna impedance and chip impedance, respectively. It is obvious from Equation (1) that when $R_a = R_c$ and X_a = -X_c, the value of power transmission coefficient reaches its maximum and equals 1. In this state, all energy is effectively transmitted between the tag antenna and tag chip without loss, and the tag antenna is resonant. However, the antenna impedance cannot perfectly match the conjugate impedance of the chip. Therefore, in the subsequent analysis, we consider the frequency corresponding to the impedance value closest to the conjugate impedance value of the chip as the resonant frequency of the tag antenna. From Equation (1), it can be concluded that the resonant frequency also corresponds to the maximum value of the power transmission coefficient.

The proposed antenna evolved from a simple structure shown in Figure 2(a). Then, the final configuration is obtained after three evolutions from Figure 2(b) to (d). The reactance and resistance curves during the evolution process are demonstrated in Figures 3(a) and (b), respectively. Furthermore, Figure 4 illustrates the curves of the power transmission coefficient.

Figure 2(a) shows the initial design of the antenna, named Antenna I, which consists of a rectangular feed ring and a pair of symmetrical dipole arms. The resistance and reactance curves of Antenna I in Figure 3 show that the impedance value $3.13 + j222.41\,\Omega$ at 1.456 GHz is closest to the complex conjugate value of the chip impedance. Meanwhile, the maximum power transmission coefficient is 0.6 at the frequency of 1.456 GHz. Based on Antenna I, a pair of L-shaped stubs are added to two symmetrical antenna arms to form Antenna II, as shown in Figure 2(b). Figures 3 and 4 show that Antenna II resonates at 1.334 GHz, with an impedance of $5.35 + j222.33\,\Omega$. Similarly, Antenna III adds another pair of larger L-shaped stubs, as shown in Figure 2(c). Antenna III further decreases the resonant frequency and improves the impedance conjugate match, significantly increasing the maximum power transmission coefficient to nearly 1 at 1.182 GHz. From Figure 2(c), it can be observed that two gaps are generated between the left and right L-shaped stubs. Then two interdigitated structures are inserted, forming Antenna IV, as shown in Figure 2(d). As observed from Figures 3 and 4, Antenna IV resonates at 0.92 GHz and keeps the maximum power transmission coefficient to nearly 1.

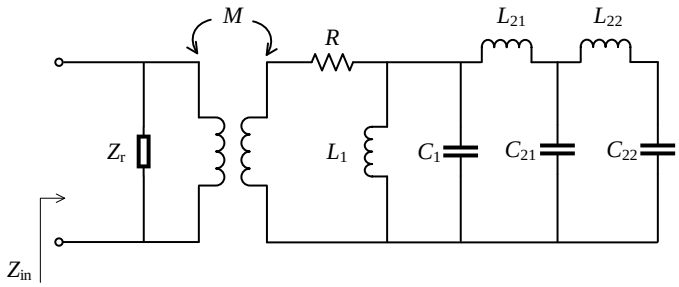

FIGURE 5. Equivalent circuit of the proposed tag antenna.

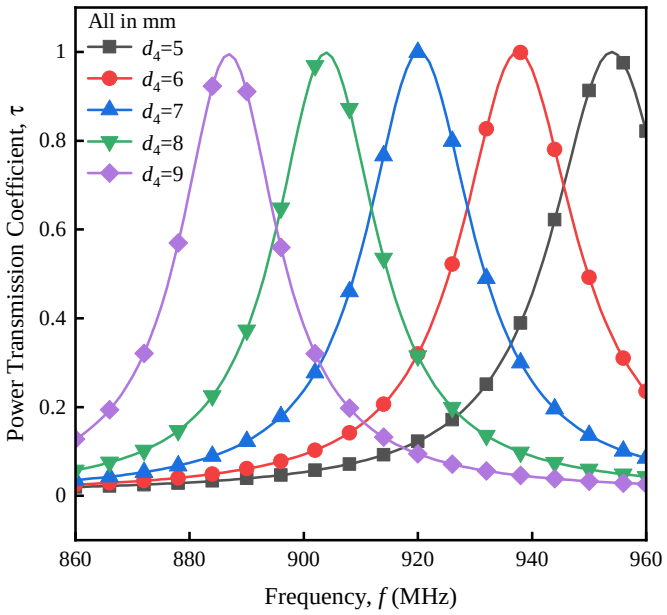

FIGURE 6. The effect of d_4 on the power transmission coefficient.

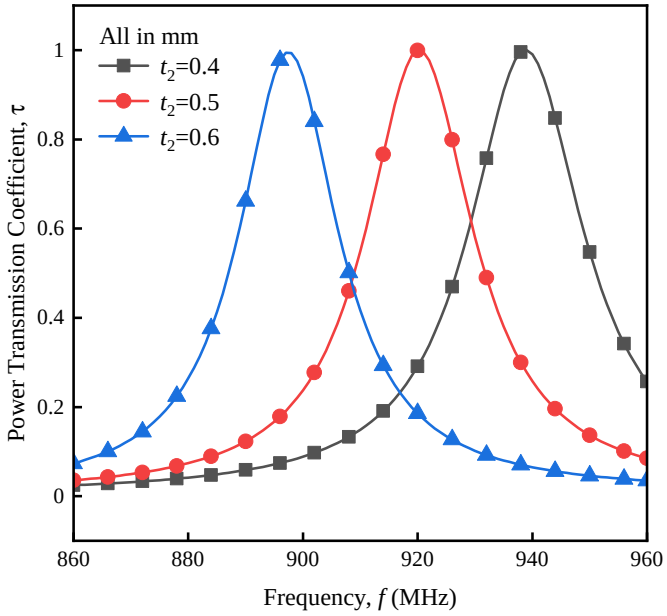

FIGURE 7. The effect of t_2 on the power transmission coefficient.

The interdigitated structure is composed of a series of staggered open stubs, as shown in Figure 1. Introducing these interdigitated structures increases the antenna's equivalent inductance and capacitance, which in turn lowers the resonant frequency and reduces the overall antenna size. In the proposed tag antenna, two interdigitated structures — Interdigitated Structure I and Interdigitated Structure II — are included, each offering different tuning capabilities. A detailed analysis of the design and tuning of the double interdigitated structures will be provided in the subsequent tuning analysis section.

2.3. Tuning Analysis

2.3.1. Equivalent Circuit of the Proposed Tag Antenna

In order to facilitate the analysis of the tuning principle of the proposed antenna, the equivalent circuit of the proposed tag antenna is modeled, as shown in Figure 5. The proposed tag antenna can be simplified as a dipole connected to a rectangular loop, with coupling between them [21]. Z_r is the equivalent impedance of rectangular loop. M represents the mutual coupling between the dipole and the rectangular loop. R is the total resistance including the radiation resistance and the equivalent resistance of dielectric loss. L_1 and C_1 are the equivalent inductance and equivalent capacitance of the dipole arms, respectively. For Interdigitated Structure I, L_{21} and C_{21} are the equivalent inductance produced by each open stub and capacitance between adjacent open stubs, respectively. For Interdigitated Structure II, the equivalent inductance (L_{22}) and capacitance (C_{22}) can also be defined in a similar manner. The resonant frequency of the equivalent circuit of an antenna can be expressed by Equation (2):

$$f = \frac{1}{2\pi\sqrt{LC}} \tag{2}$$

where L and C are the total equivalent inductance and equivalent capacitance of the antenna, respectively. Here, we focus on the capacitive effect generated by the interdigitated structures, which can be explained by Equation (3):

$$C_s = \frac{\varepsilon_0 \varepsilon_r A_e}{d} \tag{3}$$

where ε_0 is the vacuum permittivity, ε_r the relative permittivity, A_e the effective surface area, and d the spacing. Therefore, when the spacing d is reduced or the effective area A_e in-

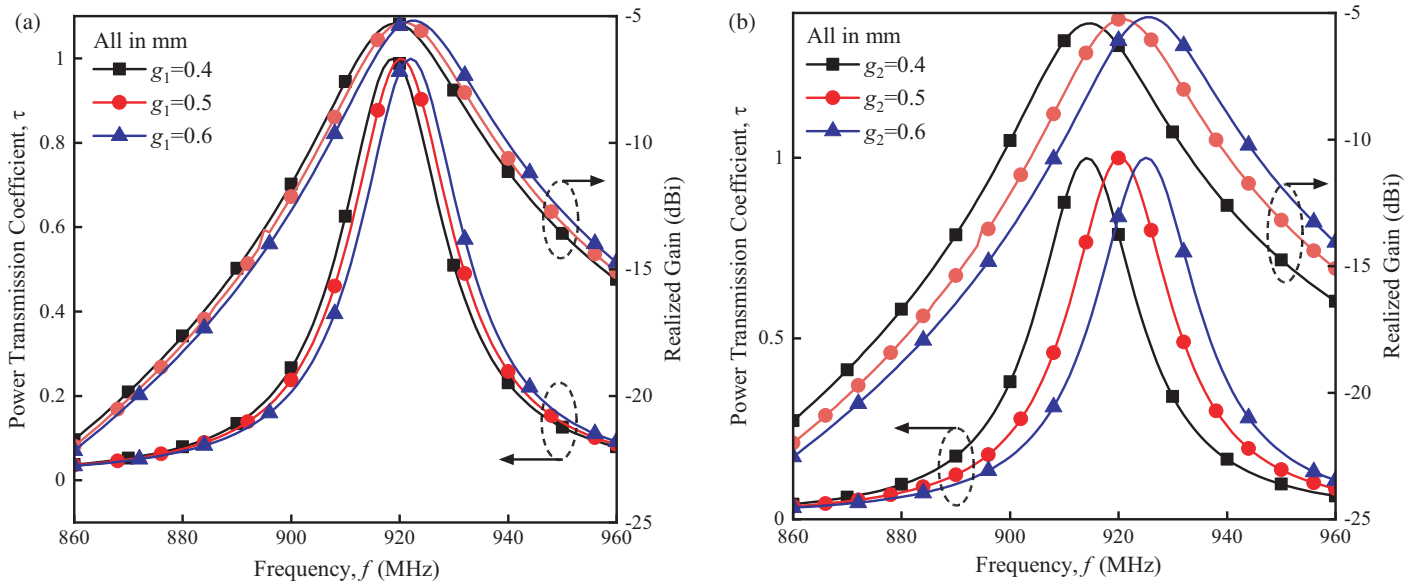

FIGURE 8. Effects of the interdigitated structure end gaps width on the power transmission coefficients and realized gains of the proposed tag antenna. (a) Parameter g_1. (b) Parameter g_2.

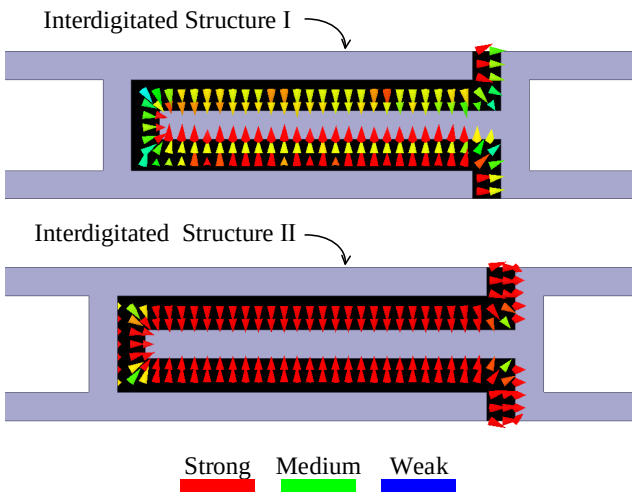

FIGURE 9. Electric field distribution of the interdigitated structure slots at 0.92 GHz.

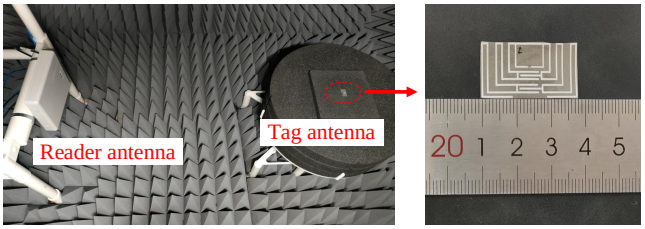

FIGURE 10. Measurement setup of Voyantic Tagformance Pro and the fabricated tag antenna.

creased, the equivalent capacitance will increase. For the double interdigitated structures in this paper, we will discuss the effects of varying structural parameters on equivalent capacitance and power transmission coefficient, then, further complete the tuning analysis in the following section.

2.3.2. Tuning Analysis of Interdigitated Structure I and Interdigitated Structure II

Figure 6 illustrates the impact of the Interdigitated Structure II length (d_4) on the power transmission coefficient. As d_4 is varied from 5 mm to 9 mm, the resonant frequency of the tag antenna gradually shifts to lower frequencies while the maximum value of the power transmission coefficient remains nearly unchanged. This can be explained from Equation (3) that when d_4 is lengthened, the effective area to generate capacitance is becoming larger, finally resulting in the resonant frequency shifting lower.

Figure 7 illustrates the impact of the stub width (t_2) on antenna performance. As t_2 is broadened from 0.4 mm to 0.6 mm, the trend observed in the power transmission coefficient curve is similar to d_4. This is because a broader stub reduces the spacing between adjacent stubs, generating larger equivalent capacitance. Therefore, the antenna's resonant frequency has a trend of down shifting.

Figures 8(a) and (b) show that the resonance of the tag antenna can also be tuned by adjusting g_1 and g_2. As the end gap width of the Interdigitated Structure I (g_1) narrows from 0.6 mm to 0.4 mm, the resonant frequency of the tag antenna decreases from 922 MHz to 919 MHz, with a tuning sensitivity of 15 MHz/mm. However, g_2 shows a tuning sensitivity of 55 MHz/mm as it decreases from 0.6 mm to 0.4 mm. This comparison demonstrates that changing g_2 achieves a coarse tuning of the tag resonant frequency, while changing g_1 is fine tuning. Differences in tuning sensitivities can be explained from the electric field distribution in Figure 9. The electric field strength of the Interdigitated Structure II is higher than that of the Interdigitated Structure I. Moreover, this tuning method only affects

TABLE 2. Various parameters comparison of the proposed antenna with few previous reported antennas.

Ref.	Tag Dimension (mm)	Size Reduction (%)	Substrate	Fabrication Complexity and Cost	Max. Read Distance (m)
This paper	28×16	-	PET	Low	6.8
[15]	53.5 × 12	30	Copper tape and foam	High	9.7
[17]	55.2 × 44.2	82	PTFE	Medium	7.0
[23]	50 × 12	25	FR4	High	6.3
[24]	30 × 26	43	Paper	High	1.5
[25]	44 × 59	83	Photo paper	Low	5.8
[26]	128.3 × 50	93	FR4	High	5.5
[27]	∼ 70 × 24	∼ 73	FR4	High	7.0

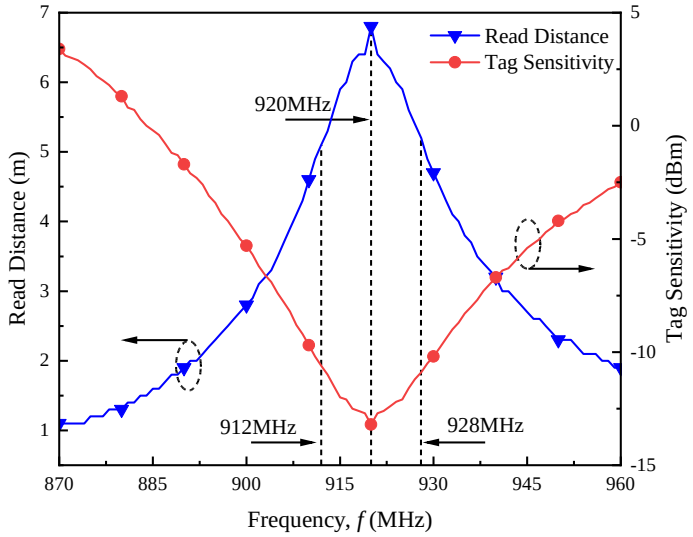

FIGURE 11. Measured tag sensitivity and measured read distance of the proposed tag antenna.

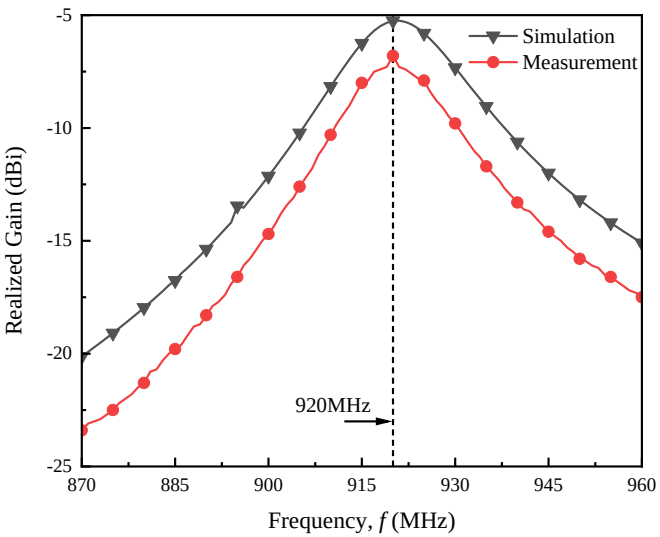

FIGURE 12. Measured and simulated realized gains of the proposed tag antenna.

the resonant frequency of the tag antenna significantly and has little effect on the maximum power transmission coefficient and peak gain, as shown in Figure 8. The relevant adjustment operation is both easy and effective, making less change on the overall configuration of the antenna than other parameters.

3. RESULTS AND DISCUSSION

According to the optimized parameters in Table 1, the proposed antenna was fabricated and tested in the anechoic chamber of Voyantic Tagformance Pro measurement system [22], as depicted in Figure 10. The tag to be tested is positioned at the center of a black foam rotating platform, while the linearly polarized reader antenna is placed at a certain distance to the tag antenna. During the measurement process, the effective isotropic radiated power (EIRP) is affixed at 3.28 W.

Figure 11 shows the measured read distance and sensitivity of the proposed tag at different frequencies. In the range of 870 ∼ 960 MHz, the tag exhibits a maximum read distance of 6.8 m at 920 MHz, and the optimal tag sensitivity is −13.2 dBm. Figure 12 depicts the simulated and measured realized gains. In simulation, the tag antenna achieves a peak realized gain of −5.3 dBi at 920 MHz. In measurement, the highest realized gain is −6.8 dBi, indicating a decrease of 1.5 dB compared to the simulated. This is because the measurement environment and simulation environment are not fully consistent, and the tag antenna also inevitably has manufacturing tolerances in the fabrication process. It can also be observed from Figures 11 and 12 that the performance deteriorates as the frequency gradually decreases or increases from 920 MHz. For example, at 912 MHz, the read distance is 5.1 m with a sensitivity of −10.6 dBm, while at 928 MHz, the read distance is 5.2 m with a sensitivity of −10.9 dBm. Figure 13 shows the antenna's read patterns in the xoy plane and xoz plane. The xoy plane is shaped like an "8" with the farthest read distance and the best sensitivity at $\phi = 180°$. The xoz plane has omnidirectional radiation, with read distances ranging from 6 m to 6.8 m and sensitivity ranging from −13.2 dBm to −12.1 dBm. The proposed antenna is also tested on the curved surface of a plastic bottle, as shown in 14(a). Figure 14(b) illustrates the corresponding reading performance, with a maximum reading distance of 5.3 m and an optimal sensitivity of −10.6 dBm.

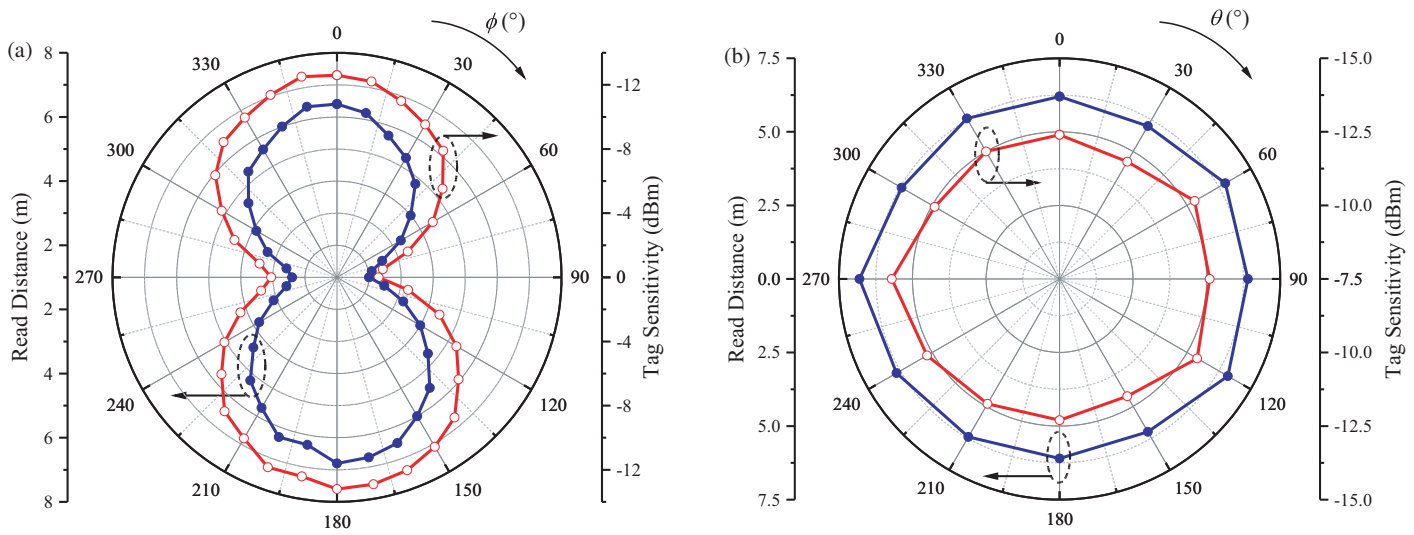

FIGURE 13. Measured read distances and tag sensitivities of the proposed tag antenna in the (a) xoy plane and (b) xoz plane.

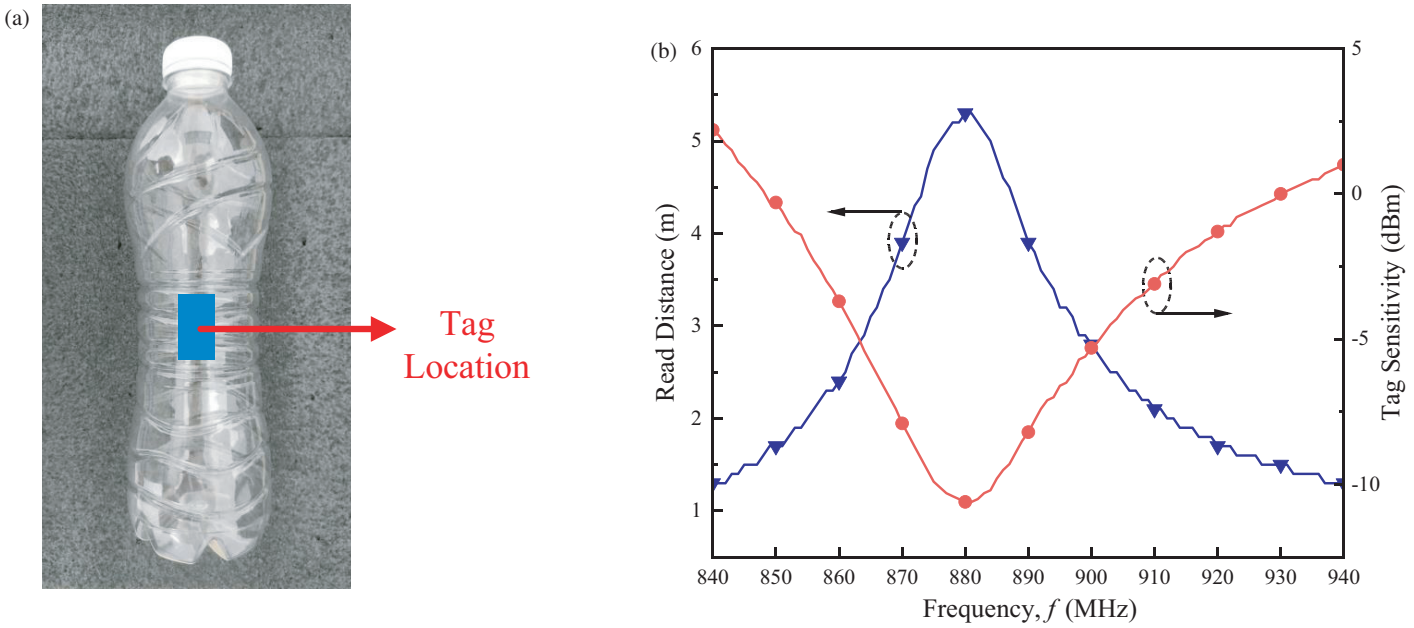

FIGURE 14. Measured read distances of the proposed tag antenna on the plastic bottle with curved surface. (a) Picture of the plastic bottle. (b) Corresponding measured read distance and tag sensitivity.

To emphasize the advantages of the proposed tag in terms of miniaturization and read distance, we compared its performance with various antennas from recent publications, as shown in Table 2. Using an EIRP of 3.28 W and a chip sensitivity of -20 dBm as standard benchmarks, the maximum read distances from the references are converted accordingly for comparison. The data in the "Size Reduction" column demonstrates the miniaturization advantage of the proposed antenna compared to other antennas. The data are calculated as Size Reduction $= (S_1 - S_2)/S_1 \times 100\%$, where S_1 represents the planar size of the tag from references, and S_2 represents the planar size of the tag antenna in this paper. Compared to the tag antennas in [23, 26, 27], the proposed antenna has the advantage of flexibility, making it suitable for more applications. Compared to the folded design in [15] and the stacked design in [24], the tag antenna proposed in this paper adopts an ultra-low profile and single-layer design, which is easier to manufacture. In terms of read distance and size, the tag antenna in this study achieves different degrees of size reduction compared to those reported in the references, while exhibiting comparable or even extended read distances. Generally, the proposed tag antenna stands out for its miniaturization, flexibility, low processing cost, and simplified fabrication.

4. CONCLUSION

A compact UHF RFID tag antenna has been proposed, fabricated, and tested in this work. The design utilizes multiple L-shaped stubs and incorporates two interdigitated structures between the left and right radiation arms to achieve miniaturization. The resonant frequency of the tag can be adjusted both coarsely and finely by varying the interdigitated structures, without significantly affecting the power transmission coefficient. Experimental measurements demonstrate that the tag antenna achieves a maximum read distance of 6.8 m at 920 MHz, with an optimal tag sensitivity of −13.2 dBm.

ACKNOWLEDGEMENT

This work was supported in part by the University-Industry Research Collaboration Program of Fujian Province, China, under Grant 2023H6004.

REFERENCES

[1] Hughes, J. D., R. Horne, N. Brabon, and J. Batchelor, "An on-body UHF RFID tag with DDRR antenna for healthcare data streaming applications," *IEEE Journal of Radio Frequency Identification*, Vol. 6, 680–687, 2022.

[2] Casula, G. A., F. Lestini, F. P. Chietera, G. Muntoni, C. Occhiuzzi, L. Catarinucci, R. Colella, G. Montisci, and G. Marrocco, "Design of on-body epidermal antenna on AMC substrate for UHF RFID in healthcare," *IEEE Transactions on Antennas and Propagation*, Vol. 72, No. 5, 4023–4035, 2024.

[3] Motroni, A., A. Buffi, P. Nepa, M. Pesi, and A. Congi, "An action classification method for forklift monitoring in industry 4.0 scenarios," *Sensors*, Vol. 21, No. 15, 5183, 2021.

[4] Rayhana, R., G. Xiao, and Z. Liu, "RFID sensing technologies for smart agriculture," *IEEE Instrumentation & Measurement Magazine*, Vol. 24, No. 3, 50–60, 2021.

[5] Pereira, E., □. Araújo, L. F. V. Silva, M. Batista, S. Júnior, E. Barboza, E. Santos, F. Gomes, I. T. Fraga, R. Davanso, D. O. d. Santos, and J. d. A. Nascimento, "RFID technology for animal tracking: A survey," *IEEE Journal of Radio Frequency Identification*, Vol. 7, 609–620, 2023.

[6] Doan, T. N. H., K. K. Nguyen, and S. X. Ta, "Dual-band dual-LP/CP antennas using combined metasurface and patch for UHF/2.45-GHz RFID readers," *IEEE Access*, Vol. 12, 78 833–78 842, 2024.

[7] Hong, J. H., C.-W. Chiu, and H.-C. Wang, "Design of circularly polarized tag antenna with artificial magnetic conductor for on-body applications," *Progress In Electromagnetics Research C*, Vol. 81, 89–99, 2018.

[8] Mohammed, A. T. and A. S. A. Jalal, "Design of a tag antenna for RFID applications," in *2022 4th International Conference on Current Research in Engineering and Science Applications (ICCRESA)*, 375–378, Baghdad, Iraq, 2022.

[9] Sultan, Q. H. and A. M. A. Sabaawi, "Design and implementation of improved fractal loop antennas for passive UHF RFID tags based on expanding the enclosed area," *Progress In Electromagnetics Research C*, Vol. 111, 135–145, 2021.

[10] Chietera, F. P., R. Colella, and L. Catarinucci, "3D-printed fractal UHF RFID tag antenna," in *2022 7th International Conference on Smart and Sustainable Technologies (SpliTech)*, 1–4, Split/Bol, Croatia, 2022.

[11] Mikhailovskaya, A., I. Yusupov, D. Dobrykh, S. Krasikov, D. Shakirova, A. Bogdanov, D. Filonov, and P. Ginzburg, "Omnidirectional miniature RFID tag," *Applied Physics Letters*, Vol. 119, No. 3, 033503, 2021.

[12] Babar, A. A., T. Bjorninen, V. A. Bhagavati, L. Sydanheimo, P. Kallio, and L. Ukkonen, "Small and flexible metal mountable passive UHF RFID tag on high-dielectric polymer-ceramic composite substrate," *IEEE Antennas and Wireless Propagation Letters*, Vol. 11, 1319–1322, 2012.

[13] Chiang, S.-M., E.-H. Lim, P.-S. Chee, Y.-H. Lee, and F.-L. Bong, "Capacitors-loaded dipolar patch antenna for UHF tag miniaturization," in *2021 IEEE International Symposium on Antennas and Propagation and USNC-URSI Radio Science Meeting (APS/URSI)*, 181–182, Singapore, 2021.

[14] Miswadi, N., N. H. A. Rahman, E.-H. Lim, S. b. Subahir, M. A. Aris, and M. Murugesh, "Embedded inductance folded-patch antenna with inclined slots for on-metal tag design," *IEEE Journal of Radio Frequency Identification*, Vol. 8, 685–694, 2024.

[15] Choudhary, A. and D. Sood, "Wideband long range compact serrated triangular patch based UHF RFID tag for metallic base environment," *IEEE Journal of Radio Frequency Identification*, Vol. 8, 643–651, 2024.

[16] Ng, W.-H., E.-H. Lim, F.-L. Bong, and B.-K. Chung, "E-shaped folded-patch antenna with multiple tuning parameters for on-metal UHF RFID tag," *IEEE Transactions on Antennas and Propagation*, Vol. 67, No. 1, 56–64, 2019.

[17] Erman, F., D. Mansour, M. Kouali, A. Shabaneh, L. Leifsson, S. Koziel, E.-H. Lim, and E. Hanafi, "Low-profile interdigitated UHF RFID tag antenna for metallic objects," *IEEE Access*, Vol. 10, 90 915–90 923, 2022.

[18] Abdelkarim, M., M. Y. Boughrara, and A. Gharsallah, "Analysis and design of a compact SSRR for passive RFID tag antenna," in *2023 20th International Multi-Conference on Systems, Signals & Devices (SSD)*, 559–563, Mahdia, Tunisia, 2023.

[19] Dai, L., Z. Xu, and J. Yuan, "A contactless testing method for parasitic capacitance of UHF RFID tag," in *2023 IEEE 6th International Conference on Electronic Information and Communication Technology (ICEICT)*, 1152–1156, Qingdao, China, 2023.

[20] Erman, F., S. Koziel, and L. Leifsson, "Broadband/Dual-band metal-mountable UHF RFID tag antennas: A systematic review, taxonomy analysis, standards of seamless RFID system operation, supporting IoT implementations, recommendations, and future directions," *IEEE Internet of Things Journal*, Vol. 10, No. 16, 14 780–14 797, 2023.

[21] Marrocco, G., "The art of UHF RFID antenna design: Impedance-matching and size-reduction techniques," *IEEE Antennas and Propagation Magazine*, Vol. 50, No. 1, 66–79, 2008.

[22] Voyantic, Ltd., "Tagformance pro measurement system manual," Finland, 2023.

[23] Bhaskar, S. and A. K. Singh, "A compact meander line UHF RFID antenna for passive tag applications," *Progress In Electromagnetics Research M*, Vol. 99, 57–67, 2021.

[24] Lertsakwimarn, K., S. Kittiwittayapong, and D. Torrungrueng, "Double-layer passive tag antenna for UHF RFID applications," in *2021 18th International Conference on Electrical Engineering/Electronics, Computer, Telecommunications and Information Technology (ECTI-CON)*, 73–76, Chiang Mai, Thailand, 2021.

[25] Islam, M. T., T. Alam, I. Yahya, and M. Cho, "Flexible radio-frequency identification (RFID) tag antenna for sensor applications," *Sensors*, Vol. 18, No. 12, 4212, 2018.

[26] Bhaskar, S. and A. K. Singh, "A dual band dual antenna with read range enhancement for UHF RFID tags," *International Jour-*

nal of RF and Microwave Computer-Aided Engineering, Vol. 29, No. 7, e21717, 2019.

[27] Kuttikattu, F. J., K. K. A. John, S. Thomas, and T. K. Mathew, "A novel RFID dipole tag with meandered arms and a modified T-match for UHF band," in *2017 International Conference on Wireless Communications, Signal Processing and Networking (WiSPNET)*, 2488–2490, Chennai, India, 2017.